GEOCHEMISTRY

Chalcogen isotopes reveal limited volatile contribution from late veneer to Earth

Wenzhong Wang[1,2,3,4]*, Michael J. Walter[3], John P. Brodholt[4,5], Shichun Huang[6], Michail I. Petaev[7]

The origin of Earth's volatile elements is highly debated. Comparing the chalcogen isotope ratios in the bulk silicate Earth (BSE) to those of its possible building blocks, chondritic meteorites, allows constraints on the origin of Earth's volatiles; however, these comparisons are complicated by potential isotopic fractionation during protoplanetary differentiation, which largely remains poorly understood. Using first-principles calculations, we find that core-mantle differentiation does not notably fractionate selenium and tellurium isotopes, while equilibrium evaporation from early planetesimals would enrich selenium and tellurium in heavy isotopes in the BSE. The sulfur, selenium, and tellurium isotopic signatures of the BSE reveal that protoplanetary differentiation plays a key role in establishing most of Earth's volatile elements, and a late veneer does not substantially contribute to the BSE's volatile inventory.

INTRODUCTION

Understanding how Earth accreted its volatile elements, particularly its life-essential elements, is key to understanding the evolution and habitability of terrestrial planets. One group of hypotheses suggests that proto-Earth accreted mainly from volatile-poor materials from the inner Solar system, with subsequent addition of volatile elements supplied by volatile-rich materials from the outer Solar system to the bulk silicate Earth (BSE) after core formation had ceased (*1*–*4*).

The late-addition model, often referred to as a "late veneer," was originally proposed to explain the abundances of highly siderophile elements (HSEs) in the BSE (*5*, *6*), as metal/silicate partitioning indicated their near complete segregation into the metal phase during Earth's core formation (*7*). This model was subsequently adopted to account for chalcogen [sulfur (S), selenium (Se), and tellurium (Te)] abundances in the BSE (*3*) because their concentrations in the Earth's mantle are much higher than expected from their metal/silicate partition coefficients (*8*, *9*). Further, mantle peridotites were found to have chalcogen/HSE abundance ratios similar to those of carbonaceous chondrites, providing evidence for the late delivery of carbonaceous chondrite–like material to Earth's mantle (*3*), although it remains debated whether the chalcogen/HSE ratios measured in peridotites are representative of the BSE's signatures given their complicated geological history (*10*). However, recent experiments suggest that S metal/silicate partition coefficients at core-forming conditions (~20 to 60 GPa and >3000 K) (*11*) are much smaller than that at low pressures, and the modeled S abundance in the BSE after core formation could even be higher than the measured value for the Earth's mantle. Thus, a late veneer is not needed to explain the S abundance, and possibly volatile elements more generally, in the BSE.

An alternative possibility is that the proto-Earth accreted from volatile-rich materials, and the present-day volatile element abundances in the BSE were set primarily by protoplanetary differentiation processes including planetesimal evaporation and core formation (*12*–*14*). Chalcogen isotopes can provide independent constraints on the origin and evolution of Earth's volatile elements. Earth's mantle has a lighter S isotope composition ($\delta^{34}S = [(^{34}S/^{32}S)_{sample}/(^{34}S/^{32}S)_{std} - 1] \times 1000$, where std. refers to the standard sample) than any type of chondritic meteorite (fig. S1) (*15*, *16*), whereas its Se and Te isotopic compositions ($\delta^{82/76}Se = [(^{82}Se/^{76}Se)_{sample}/(^{82}Se/^{76}Se)_{std} - 1] \times 1000$; $\delta^{128/126}Te = [(^{128}Te/^{126}Te)_{sample}/(^{128}Te/^{126}Te)_{std} - 1] \times 1000$) are similar to those of carbonaceous chondrites but significantly heavier than those of enstatite chondrites (*17*–*19*), a postulated dominant isotopic component of Earth's building materials (*20*).

The subchondritic $\delta^{34}S$ of the BSE, which cannot be a result of a late veneer, is plausibly explained by evaporation from molten planetesimals, with negligible S isotope fractionation during core formation (*21*). This suggests that protoplanetary differentiation may have played a key role in establishing Earth's volatile element inventory (*12*–*14*), rather than a late veneer. In contrast, the similarity in $\delta^{82/76}Se$ between the BSE and carbonaceous chondrites was argued to be the result of the late addition of carbonaceous chondrite–like material to Earth (*17*), which can also explain the $\delta^{128/126}Te$ of the BSE (*19*). Such a conclusion can be drawn only if protoplanetary differentiation processes did not fractionate Se and Te isotopes. However, Se and Te have cosmochemical and geochemical characteristics similar to S (*22*, *23*), and it is important to assess their isotope fractionation during evaporation and core formation.

RESULTS

Structural properties of Se and Te in melts

We conducted first-principles calculations (see details in Materials and Method) to obtain the equilibrium Se and Te isotope fractionation factors between silicate and metal and between vapor and

[1]Deep Space Exploration Lab/School of Earth and Space Sciences, University of Science and Technology of China, Hefei, Anhui 230026, China. [2]CAS Center for Excellence in Comparative Planetology, University of Science and Technology of China, Hefei, Anhui 230026, China. [3]Earth and Planets Laboratory, Carnegie Institution for Science, Washington, DC 20015, USA. [4]Department of Earth Sciences, University College London, London WC1E 6BT, UK. [5]Centre of Planetary Habitability, University of Oslo, Oslo, Norway. [6]Department of Earth and Planetary Sciences, University of Tennessee, Knoxville, TN 37996, USA. [7]Department of Earth and Planetary Sciences, Harvard University, Cambridge, MA 02138, USA.
*Corresponding author. Email: wwz@ustc.edu.cn

silicate. Selenium and Te are redox-sensitive elements, but there is no literature study investigating the Se and Te species in silicate melts under different redox conditions. By analogy to S, which predominantly occurs as S^{2-} at log fO_2 < FMQ − 1 [1 log unit lower than the fayalite-magnetite-quartz (FMQ) buffer] in silicate melts (*24*, *25*), the Se and Te species are likely dominated by Se^{2-} and Te^{2-} in silicate melts at the fO_2 conditions of core formation for Earth (log fO_2 < FMQ − 4) (*26*, *27*), respectively. We model the silicate melts using $Mg_{32}Si_{32}O_{95}Se$, $Mg_{30}NaCa_2Fe_4Si_{24}Al_3H_2O_{89}Se$ (model "pyrolite"), and $Mg_{30}NaCa_2Fe_4Si_{24}Al_3H_2O_{89}Te$ compositions. The metallic melts are modeled by two multicomponent alloys, $Fe_{87}Ni_4Si_{10}C_2O_2H_2S_2Se$ and $Fe_{87}Ni_4Si_{10}C_2O_2H_2S_2Te$.

The structures of Se-bearing melts at 5 to 100 GPa and 3000 K were derived from first-principles molecular dynamics (FPMD) simulations. The FPMD results show that Se is mainly bonded to Mg and Si atoms in $Mg_{32}Si_{32}O_{95}Se$ melt with a Se—Si distance of 2.25 to 2.29 Å and a Se—Mg distance of 2.47 to 2.57 Å (fig. S2; see details in the Supplementary Materials), while it is primarily bonded to Fe atoms with a Se—Fe distance of ~2.2 Å in $Mg_{30}NaCa_2Fe_4Si_{24}Al_3H_2O_{89}Se$ melt (fig. S3). In $Fe_{87}Ni_4Si_{10}C_2O_2H_2S_2Se$ metallic melt, Se is dominantly bonded to Fe atoms with a Se—Fe distance of 2.20 to 2.30 Å (fig. S4). Similarly, Te is also mainly bonded to Fe atoms in $Mg_{30}NaCa_2Fe_4Si_{24}Al_3H_2O_{89}Te$ and $Fe_{87}Ni_4Si_{10}C_2O_2H_2S_2Te$ melts (fig. S5). The bonding configurations of Se and Te in silicate and metallic melts are similar to those of S under relatively reducing conditions (*21*).

Equilibrium Se and Te isotope fractionation between silicate and metallic melts

The average force constants, <F>, of Se and Te in melts are controlled by their bonding structures and were calculated using snapshots from the FPMD simulations based on the harmonic approximation (see Materials and Methods). The <F> of Se in $Mg_{32}Si_{32}O_{95}Se$ melt increases from ~133 N/m at 5 GPa to ~365 N/m at 82 GPa (fig. S6) because the coordination numbers of Se—Si and Se—Mg bonds substantially increase with pressure (fig. S2). The <F> of Se in $Mg_{30}NaCa_2Fe_4Si_{24}Al_3H_2O_{89}Se$ melt falls on the <F> versus pressure trend of $Mg_{32}Si_{32}O_{95}Se$ melt, suggesting a negligible compositional effect on <F> of Se in silicate melts (fig. S6). Similarly, the <F> of Se in the metallic melt increases by ~1.6 times from 11 to 100 GPa due to the considerable increase in the coordination number of the Se—Fe bond with compression (fig. S4). However, the <F> difference between silicate and metallic melts does not notably change with pressure, which is only 5 to 25 N/m at 10 to 80 GPa (fig. S6). The <F> difference of Te between $Mg_{30}NaCa_2Fe_4Si_{24}Al_3H_2O_{89}Te$ and $Fe_{87}Ni_4Si_{10}C_2O_2H_2S_2Te$ melts is <10 N/m at ~44 GPa. For comparison, the <F> difference of S between the reducing silicate melt and the metallic melt is <30 N/m at <80 GPa (*21*).

The equilibrium fractionation value ($10^3\ln\alpha_{silicate\text{-}metal}$) of $^{82/76}Se$ and of $^{128/126}Te$ between silicate and metallic melts is derived from the <F> differences using the high-temperature approximation of the Bigeleisen-Mayer equation (see the Supplementary Materials) (*28*). The silicate melt is only marginally enriched in heavy Se and Te isotopes relative to the metallic melt. For example, at 3000 K, the $10^3\ln\alpha_{silicate\text{-}metal}$ of $^{82/76}Se$ is <+0.012 ‰ at 10 to 60 GPa (Fig. 1), and the $10^3\ln\alpha_{silicate\text{-}metal}$ of $^{128/126}Te$ is essentially zero at ~44 GPa.

We further model the Se and Te isotope fractionation during Earth's core formation using two endmember models, equilibrium and Rayleigh distillation models. Residual Se and Te abundances in the BSE after core formation are determined by their metal-silicate partition coefficients. Previous experiments (*8*) report a large Se partition coefficient (up to ~120 at 3000 K) between silicate and metal ($D_{Se}^{metal/silicate}$) at low pressures (<20 GPa), which is similar to the silicate-metal S partition coefficient ($D_S^{metal/silicate}$). However, subsequent experiments (*29*) at >40 GPa suggest that S becomes much less siderophile at Earth's core-forming conditions than previously estimated from extrapolation of low-pressure data (*8*). If this applies to Se, then $D_{Se}^{metal/silicate}$ would also be smaller than the low-pressure data at Earth's core-forming conditions. Given this uncertain behavior at high pressures, we model a large range of $D_{Se}^{metal/silicate}$ (30 to 120). Our results show that core-mantle differentiation can only shift the BSE's $\delta^{82/76}Se$ by at most +0.01 and + 0.05‰ for equilibrium and Rayleigh distillation models (Fig. 1), respectively, indicating that core formation cannot explain the BSE's $\delta^{82/76}Se$ if Earth accreted predominantly from enstatite chondrite–like material (*20*). Similarly, core formation can only shift the BSE's $\delta^{128/126}Te$ by at most +0.005‰ even if $D_{Te}^{metal/silicate}$ is ~300 and $\delta^{34}S$ by <+0.1 ‰ (*21*), which cannot explain the $\delta^{34}S$ difference between the BSE and enstatite chondrites.

Isotope fractionation during planetesimal evaporation

We now consider the effect of evaporative loss from molten planetesimals that formed proto-Earth. Previous studies (*30*, *31*) suggest that the net isotope fractionation between vapor and melt during planetesimal evaporation strongly depends on the evaporative conditions (*30*), e.g., the vapor pressure or the degree of vapor saturation. If the degree of vapor saturation is far lower than 100%, the kinetic effect dominates the net isotope fractionation (*30*, *31*), and the residual melt is always enriched in heavy isotopes after evaporation. This might plausibly explain the heavy $^{82/76}Se$ ratio in the BSE relative to enstatite chondrite–like material (*17*), but it cannot explain the BSE's negative $\delta^{34}S$ value relative to chondrites (*15*, *16*).

When planetesimals undergo evaporation in the presence of nebular H_2 under a total pressure of ~10^{-4} bar, the vapor saturation degree approaches 100%, and the net isotope fractionation is equal to the equilibrium isotope fractionation between vapor and melt ($10^3\ln\alpha_{vapor\text{-}silicate}$) (*30*, *31*). Our previous thermodynamic calculations using the GRAINS code show that S mainly occurs as H_2S in the vapor phase (Fig. 2), which is enriched in heavy S isotopes relative to the silicate melt (*21*). Modeling indicates that the subchondritic $\delta^{34}S$ signature in the BSE can be explained by the evaporative loss of ~90% S mainly as H_2S from molten planetesimals due to the positive $10^3\ln\alpha_{vapor\text{-}silicate}$ of S isotopes (Fig. 2D).

Following the framework for S isotopes, we conducted thermodynamic calculations with solar abundances (*22*) under $1e^{-4}$ bar using GRAINS to determine the Se and Te species in the vapor phase. The results show that Se in the vapor phase mainly occurs as atomic Se (g), whose fraction increases from ~83% at 1300 K to ~97% at 1500 K (Fig. 2A). The dominant species for Te in the vapor phase is also atomic Te (g), whose fraction is >99% at 1300 to 1500 K. In contrast, S in the vapor phase mainly occurs as H_2S (g) and/or HS (g) at 1300 to 1500 K (Fig. 2B). The different species for Se and S in the vapor phase reflect a higher electronegativity for S, leading to a negative Gibbs free energy of formation of H_2S (g), whereas the Gibbs free energy of formation is positive for H_2Se (g) and H_2Te (g) (fig. S7). That is, at 1300 to 1500 K and 10^{-4} bar total

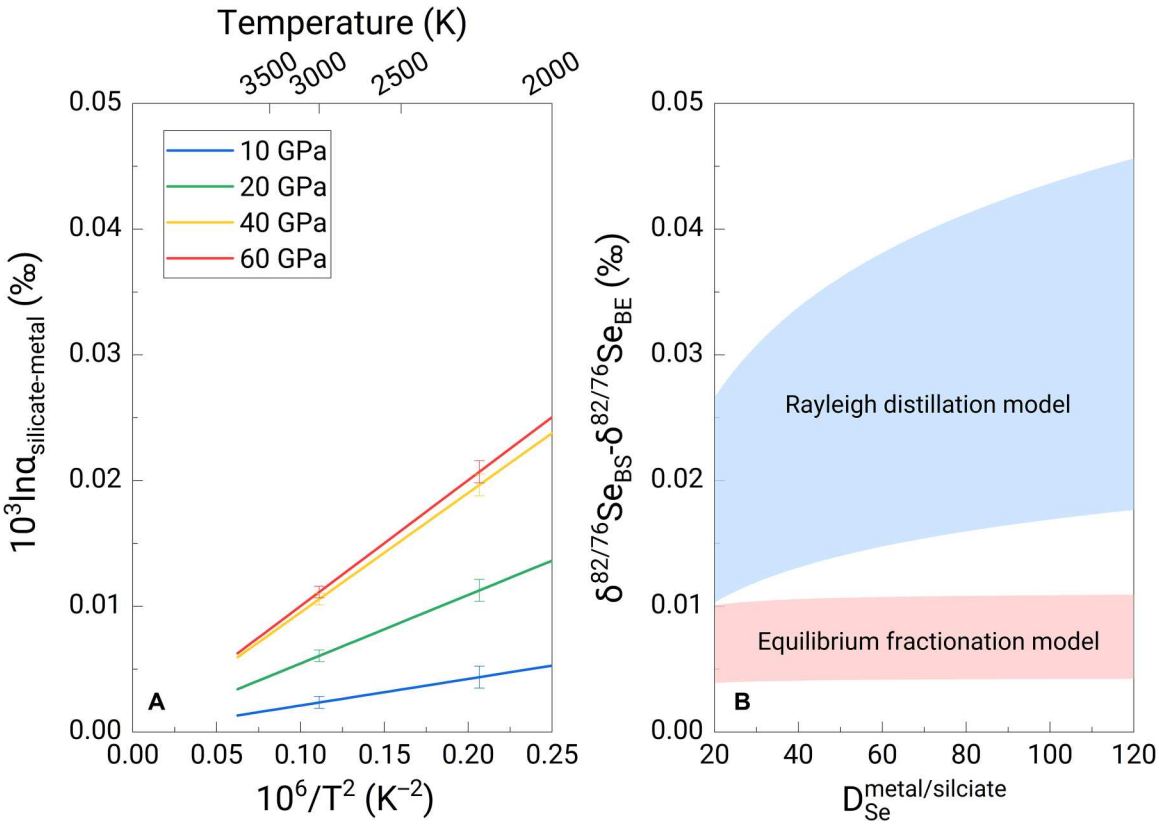

Fig. 1. Selenium isotope fractionation during core formation. (**A**) Equilibrium Se isotope fractionation factors ($10^3 \ln\alpha$ of $^{82/76}Se$) between silicate and metallic melts. Error bars represent ±1σ deviation derived by the propagation of ±1σ deviation on the force constant. (**B**) Modeled $\delta^{82/76}Se$ difference between the bulk silicate part ($\delta^{82/76}Se_{BS}$) and the bulk Earth ($\delta^{82/76}Se_{BE}$) caused by mantle-core differentiation. The Se partition coefficient ($D_{Se}^{metal/silicate}$) determines the remaining Se fraction in the silicate part after core formation. Equilibrium and Rayleigh distillation models are considered as two endmember models.

pressure, H_2S (g) is a stable phase, but H_2Se (g) and H_2Te (g) are not. We also conducted thermodynamic simulations with solar elemental abundances, but the H concentration decreased by one order of magnitude, which corresponds to a more oxidizing condition than the solar nebula. The results show that the fractions of major Se and Te species in the vapor phase do not substantially change compared with the foregoing case (see Supplementary Materials).

To determine the $10^3 \ln\alpha_{vapor\text{-}silicate}$, we conducted first-principles calculations to derive the <F> in all species and estimated the <F> in the vapor phase based on their fractions. The vapor phase is enriched in light Se and Te isotopes relative to the silicate melt with the $10^3 \ln\alpha_{vapor\text{-}silicate}$ of $^{82/76}Se$ ranging from −0.1 to −0.2‰ and the $10^3 \ln\alpha_{vapor\text{-}silicate}$ of $^{128/126}Te$ from −0.031 to −0.023‰ at 1300 to 1500 K (Fig. 2C and fig. S8). Thus, Se and Te isotopes show an opposite fractionation direction to that of S (Fig. 2D), such that evaporative loss of S, Se, and Te from molten planetesimals will enrich the residual melt with light S isotopes but heavy Se and Te isotopes.

DISCUSSION

Combining the isotope fractionation data from our study and the literature metal/silicate partition coefficients (*8*, *9*, *29*), we model the abundances and isotopic compositions of S, Se, and Te in the BSE after early planetesimal evaporation followed by late-stage core formation.

The nature of Earth's building materials, which is required to estimate the initial abundances and isotopic compositions of S, Se, and Te, remains highly debated. Dauphas (*20*) used a large database to model the isotopic evolution of multiple elements (including O, Ca, Ti, Cr, Ni, Mo, Ru, and Nd) in Earth's mantle and found the best match if Earth accreted from materials dominated by enstatite chondrite–like (~71%) and ordinary chondrite-like (~24%) compositions, with relatively minor contributions from carbonaceous chondrite–like material (~5%). That is, Earth's accreting materials originate from both CC (carbonaceous) and NC (noncarbonaceous) reservoirs, which is also supported by Earth's nucleosynthetic K and Zn isotope anomalies (*32*–*35*). In addition, the mass-independent Mo and Nd isotopic composition of Earth's mantle may reflect a mixture between NC and unsampled *s*-process–enriched CC material compared to known chondrites (*36*–*38*). In contrast, Schiller *et al.* (*39*) found that the mass-independent $\mu^{54}Fe$ of Earth's mantle overlaps with the value of CI chondrite but is lower than other chondrites, indicating that most of Fe in Earth's mantle derived from inward-drifting CI-like material. If so, large fractions of Cr and Ni in Earth's mantle would also be delivered by the same material, but this is inconsistent with Earth's Ni and Cr isotopic signatures (*40*–*43*). We use the Dauphas model in this study as our baseline for Earth's building materials because it provides a

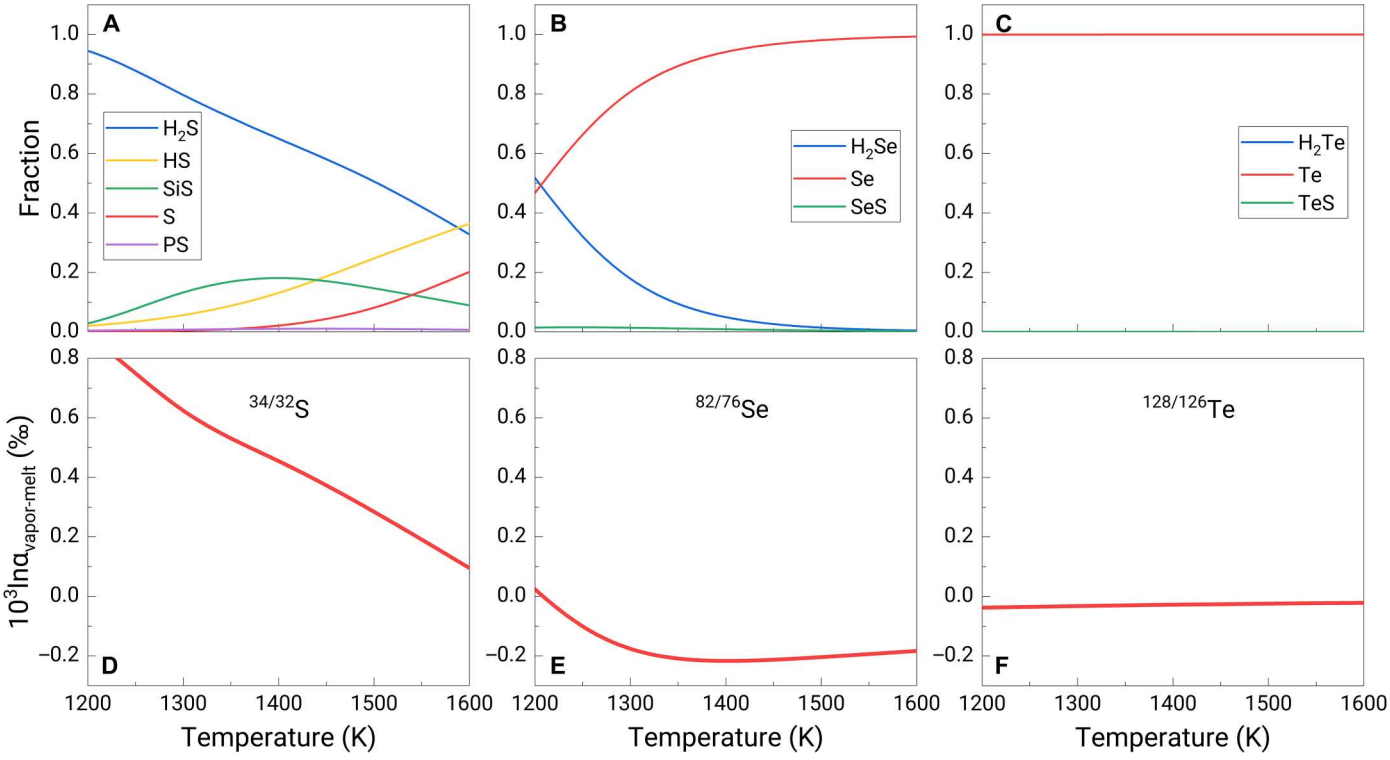

Fig. 2. Sulfur, selenium, and tellurium species in the vapor phase and the isotope fractionation between vapor and melt. (**A** to **C**) the fractions of S, Se, and Te species in the vapor evaporated from molten planetesimals with the presence of nebular H_2. At 1300 to 1500 K, Se and Te predominantly occur as Se (g) and Te (g), respectively, while S mainly occurs as H_2S (g). (**D** to **F**) the equilibrium S, Se, and Te isotope fractionation factors between vapor and melt. The residual melt is enriched in light S isotopes and heavy Se and Te isotopes relative to the vapor phase due to the different species of S, Se, and Te in the vapor phase.

plausible mixture of components based on well-defined isotopic signatures for many refractory elements.

The initial $\delta^{34/32}S$, $\delta^{82/76}Se$, and $\delta^{128/126}Te$ of Earth's building material are estimated to be ~−0.21, −0.35, and +0.02‰, respectively. The initial S, Se, and Te abundances in the accreting material are ~4.5 wt %, 20 ppm (*3*), and 1.8 ppm (*18*, *19*), respectively. Our models show that approximately 85 to 95% early evaporative loss can reproduce the present-day BSE's $\delta^{34/32}S$, $\delta^{82/76}Se$, and $\delta^{128/126}Te$, as well as the S, Se, and Te abundances after core formation over the modeled $D_S^{metal/silicate}$, $D_{Se}^{metal/silicate}$, and $D_{Te}^{metal/silicate}$ ranges, without the need for a late veneer (Fig. 3).

If the evaporative loss of S, Se, and Te is greater than 95%, then the BSE would have S, Se, and Te abundances lower than the present-day BSE's values after core formation, and its $\delta^{34/32}S$, $\delta^{82/76}Se$, and $\delta^{128/126}Te$ would deviate from the current BSE's values. In this case, a late veneer is required to increase the S, Se, and Te abundances to the level of the current BSE, but the final $\delta^{34/32}S$, $\delta^{82/76}Se$, and $\delta^{128/126}Te$ of the BSE would also be affected by the late-veneer material. To evaluate the late-veneer effect on the $\delta^{34/32}S$, $\delta^{82/76}Se$, and $\delta^{128/126}Te$ of the bulk silicate reservoir, we conduct Monte Carlo simulations with a late veneer characterized by carbonaceous chondrite–like material. The models show that the $\delta^{82/76}Se$ and $\delta^{128/126}Te$ of the BSE can always be reproduced, no matter how much Se and Te in the present-day BSE was added by a late veneer (fig. S9). However, the $\delta^{34/32}S$ of the BSE will be close to the late-veneer value if the amount of S added by the late veneer is too high, and no more than ~30% of the present-day BSE's S budget is allowed to be added by the late veneer to reproduce the BSE's $\delta^{34/32}S$ (fig. S9).

Our modeling suggests that the abundances and isotope compositions of S, Se, and Te in the BSE can be explained by protoplanetary differentiation rather than a late veneer. Although a late veneer is allowed, the amounts of S, Se, and Te added by the late veneer should not exceed ~30% of the present-day BSE's budgets. If the late-veneer volatile-rich material is sourced from the outer Solar System, e.g., carbonaceous chondrite (*1*–*4*), our result constrains that the mass of late veneer cannot exceed 0.2% of the mass of Earth's mantle. This allows an estimate of the maximum budgets of other volatile elements delivered along with chalcogens by the late veneer. Using the elemental abundances in carbonaceous chondrite (*3*, *44*–*46*) and the BSE (*47*), we find that the late veneer contributes at most 5% of the H and 40% of the C in the current BSE (*45*, *47*–*49*). The limited amount of H contributed by a late veneer indicates that Earth obtained most of its water during early accretion and differentiation (*50*) from its major building block—enstatite chondrite–like material (*51*), inherited possibly through the interaction between primordial hydrogen-rich atmosphere and proto-Earth (*52*). Further, the allowed mass of late veneer would not substantially contribute to the budgets of moderately volatile elements in the BSE, which is supported by the mass-dependent Zn and Cu isotopic signatures of Earth's mantle (*53*, *54*).

In contrast, the maximum mass of late veneer constrained from S, Se, and Te isotopes can supply 100% of the N in the current BSE [2.2 ± 1.2 ppm, (*45*, *47*, *55*)]. The pre–late-veneer BSE would have a

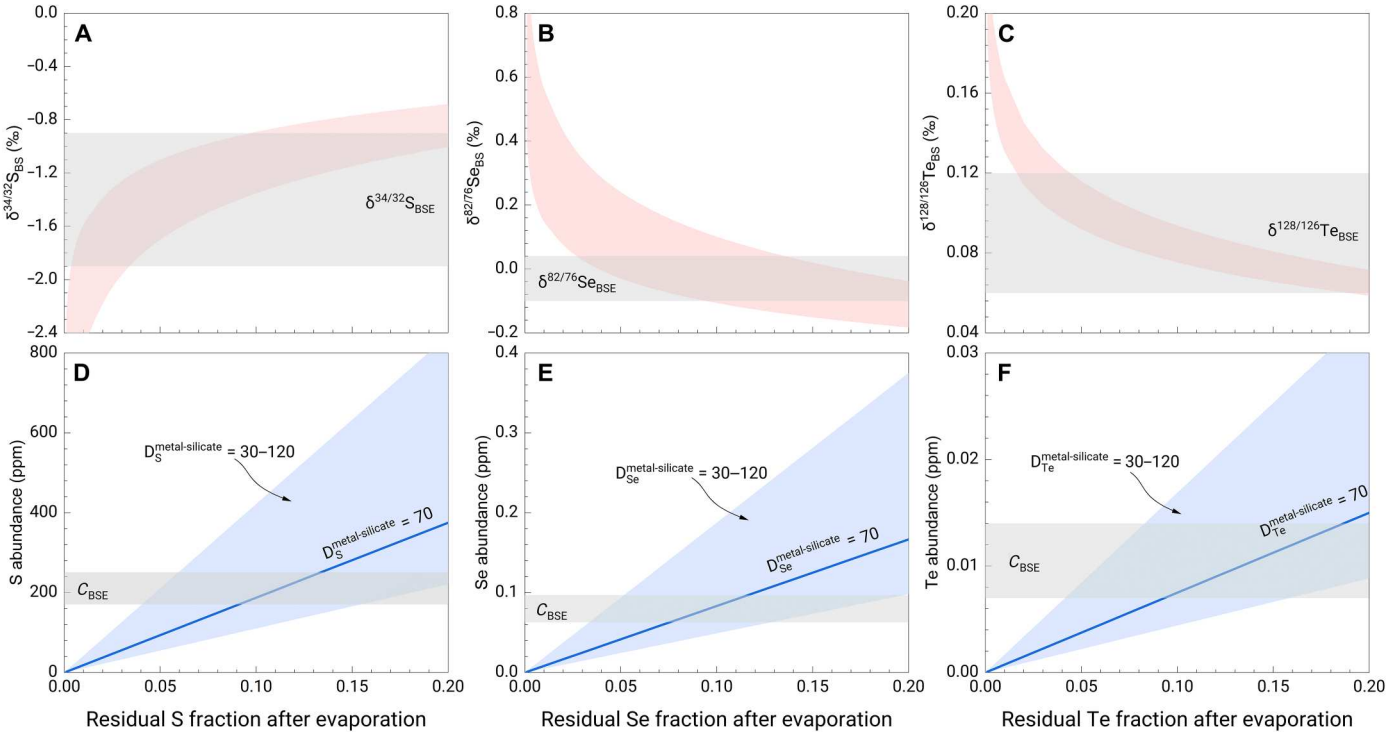

Fig. 3. Abundances and isotopic compositions of S, Se, and Te in the bulk silicate part established by planetesimal evaporation followed by core formation. The Se and Te isotopic compositions of the BSE were inferred from mantle peridotites (*17*, *19*). The previous estimate of BSE's $\delta^{82/76}$Se from mid-ocean ridge basalts (*10*) is consistent with the value from peridotites within uncertainties. (**A**) $\delta^{34/32}S_{BS}$, (**B**) $\delta^{82/76}Se_{BS}$, and (**C**) $\delta^{128/126}Te_{BS}$ as a function of the residual fraction after evaporation, as core formation does not induce resolvable S, Se, and Te isotope fractionation. The initial $\delta^{34/32}$S, $\delta^{82/76}$Se, and $\delta^{128/126}$Te of the building material (71% enstatite chondrite + 24% ordinary chondrite + 5% carbonaceous chondrite) (*20*) are estimated to be ~ −0.21, −0.35, and +0.02‰ (fig. S1), respectively. (**D**) S, (**E**) Se, and (**F**) Te abundances in the bulk silicate part after evaporation followed by core-mantle differentiation. The initial S, Se, and Te abundances in the build material are set as ~4.5 wt %, 20 ppm (*3*), and 1.8 ppm (*18*, *19*), respectively. The blue shades represent the modeled results with $D_S^{metal/silicate}$, $D_{Se}^{metal/silicate}$, and $D_{Te}^{metal/silicate}$ ranging from 30 to 120 (*8*, *9*, *29*), in which the results at $D_S^{metal/silicate}$, $D_{Se}^{metal/silicate}$, and $D_{Te}^{metal/silicate}$ ~ 70 are highlighted by the blue lines.

higher C/N ratio than the present-day BSE, which is also supported by metal-silicate partition coefficients (*14*, *56*). In addition, at most, 30% of the HSEs in the current BSE were added by a late veneer. This is consistent with recent experiments (*57*, *58*) yielding low metal-silicate partition coefficients for Pd and Pt and hinting for possible higher concentrations of platinum-group elements in the mantle after core formation. The contribution of a late veneer in establishing high abundances of other HSEs in the BSE can be independently assessed by further research on the metal-silicate partition coefficients of these HSEs under the conditions of core formation for Earth. Overall, our results show that protoplanetary differentiation may play a dominant role in establishing Earth's most volatile element inventory, and the late veneer would have a limited contribution to the BSE's volatiles, with the possible exception of N.

MATERIALS AND METHODS

Equilibrium isotope fractionation factor

The reduced partition function ratio (β) of element X in phase A, which represents the equilibrium isotope fractionation factor of element X between phase A and an ideal gas of X atoms, can be derived from the Bigeleisen-Mayer equation (*28*). On the basis of the harmonic approximation and the Teller-Redlich rule (*59*), the Bigeleisen-Mayer equation can be written as

$$\beta = \frac{Q_h}{Q_l} = \prod_i^{3N} \frac{u_{ih}}{u_{il}} \frac{e^{-\frac{1}{2}u_{ih}}}{1-e^{-u_{ih}}} \frac{1-e^{-u_{il}}}{e^{-\frac{1}{2}u_{il}}} \quad (1)$$

where h and l represent the heavy and light isotopes, respectively, and Q_h and Q_l refer to the vibrational partition function for the heavy and light isotopes, respectively. The running index i refers to the vibrational frequency mode, and N is the number of atoms in the unit cell. Parameters u_{ih} and u_{il} are defined as $u_{ih\ or\ il} = \hbar\omega_{ih\ or\ il}/k_BT$, where $\omega_{ih\ or\ il}$ is the vibrational frequency and T is the temperature in Kelvin. $\hbar$ and k_B are the reduced Planck and Boltzmann constants, respectively.

Under the high-temperature approximation, the β factor can be expressed as

$$\beta = 1 + \left(\frac{1}{m} - \frac{1}{m'}\right) \frac{\hbar^2}{8{k_B}^2T^2} \langle F \rangle \quad (2)$$

where m and m' refer to the light and heavy isotopes, respectively. $\langle F \rangle$ is the force constant of the atom of interest. Thus, the equilibrium isotope fractionation factor ($10^3\ln\alpha$) between phases A and B

can be derived from

$$10^3 \ln\alpha_{A-B} = 10^3 \ln\beta_A - 10^3 \ln\beta_B = \left(\frac{1}{m} - \frac{1}{m'}\right) \frac{\hbar^2}{8k^2T^2} (\langle F\rangle_A - \langle F\rangle_B) \quad (3)$$

Equation 3 has been also successfully applied to predict the equilibrium barium isotope fractionation between minerals and aqueous solution at low temperatures (*60*) and the S and nickel isotope fractionation between silicate and metallic melts (*21*, *42*).

First-principle molecular dynamics simulations

We calculated equilibrium Se isotope fractionation factors between silicate and metallic melts using Eq. 2. To obtain the structures of Se-bearing silicate and metallic melts, we conducted FPMD simulations based on density functional theory using Vienna Ab initio Simulation Package (VASP) with the projector-augmented wave method (*61*). The generalized-gradient approximation (*62*) was selected to describe the exchange-correlation functional and the PBE pseudopotentials were used. The energy cutoff for the plane wave was set as 600 eV, and the Brillouin zone summations over the electronic states were performed at the gamma point. We used the *NVT* thermodynamic ensemble to perform all FPMD simulations with a fixed temperature of 3000 K, which is controlled by a Nosé thermostat. The time step is 1 fs, and the total simulation time is ~60 ps. The initial melt structures were obtained by melting the starting configurations at 6000 K for 20 ps. Pressures can be derived by averaging the pressure over time after equilibration.

We first conducted FPMD simulations on silicate melts with a chemical composition of $Mg_{32}Si_{32}O_{95}Se$, in which Se has a valence state of −2. Selenium is a redox-sensitive element with four valence states: −2, 0, +4, and +6. Until now, there is no study in the literature investigating the Se species in silicate melts at variable fO_2 conditions. Previous experiments show that S^{2-} is the dominant species in silicate melts at log fO_2 < FMQ − 1 (1 log unit lower than the FMQ buffer) (*24*, *25*). By analogy to S, the dissolved Se species in silicate melts could be also dominated by Se^{2-}, at least under redox conditions of core formation for Earth, Mars, and Moon (log fO_2 < FMQ − 4) (*26*, *27*). The chemical composition of $MgSiO_3$ was chosen for silicate melts because it has similar MgO and SiO_2 contents to primitive chondrites. To check the effect of melt composition on the calculated results, we also performed FPMD simulations on a pyrolitic melt with a chemical formula of $Mg_{30}NaCa_2Fe_4Si_{24}Al_3H_2O_{89}Se$. For metallic melts, we used a multicomponent alloy ($Fe_{87}Ni_4Si_{10}C_2O_2H_2S_2Se$) to do the simulations. We did not introduce a Hubbard U correction for Fe atoms in our calculations, as previous calculations suggest that a +U correction does not substantially affect the calculated results (*63*). The pressures from FPMD simulations on Se-bearing melts range from ~5 to 100 GPa. Similar to Se, we also performed FPMD simulations on $Mg_{30}NaCa_2Fe_4Si_{24}Al_3H_2O_{89}Te$ and $Fe_{87}Ni_4Si_{10}C_2O_2H_2S_2Te$ melts at 3000 K to constrain the equilibrium Te isotope fractionation factor between silicate and metallic melts.

The structural properties of melts can be inferred from the radial distribution function (RDF). The RDF between two species A and B was calculated from

$$g_{A-B}(r) = \frac{N}{\rho N_A N_B} \left\langle \sum_{i=1}^{N_A} \sum_{j=1}^{N_B} \delta(\vec{r} - \vec{R}_i^A + \vec{R}_j^B) \right\rangle \quad (4)$$

where A and B refer to two species of interest, N is the total number of atoms, ρ is the atomic number density, and N_A and N_B refer to the total number of species A and B atoms, respectively. $\vec{R}$ represents the coordinates of these atoms. The coordination number, which represents the number of B atoms that are distributed around A atoms, can be derived from the RDF.

To obtain the <F> of Se and Te in melts, we extracted large numbers of snapshots from the FPMD trajectories every 250 steps after equilibration and relaxed the Se and Te atomic positions in each snapshot. Then, we applied seven different small displacements to the Se and Te atomic positions along each direction and calculated the energies of these strained configurations. The force constant matrix of Se and Te can be obtained by fitting the relationship between static energies and small displacements with a second-order polynomial, and the <F> of Se and Te in each snapshot is the average value of diagonal elements of the force constant matrix. The statistical average on all snapshots is the average <F> in melts (fig. S6).

Vapor-melt se and Te isotope fractionation

Estimating the Se and Te isotope fractionation between vapor and melt during planetesimal evaporation requires understanding the Se and Te species in the vapor phase. Similar to previous work on S species (*21*), we conducted thermodynamic calculations using the GRAINS code (*64*) with solar abundance for the elements (*22*) at various temperatures and $1e^{-4}$ bar. This code calculates the minimum Gibbs free energy of a given system and outputs all the species when the system achieves chemical equilibrium. The conditions adopted here correspond to the case that the solar nebular would not have completely dissipated during planetesimal evaporation in the first several million years (*65*). Also, planetesimal evaporation in the presence of nebular H_2 is key to explaining the subchondritic $\delta^{34}S$ signature of the BSE (*21*). To check the effect of H concentration on the Se and Te species in the vapor phase, we also conducted thermodynamic calculations with solar elemental abundances but with H concentration decreased by one order of magnitude, conditions that are more oxidizing than the solar nebular.

We further calculated the <*F*> of Se and Te in all these species using first-principle calculations. The atomic positions of molecules in a cubic box (20 Å by 20 Å by 20 Å) were relaxed, and then the <*F*> was derived using the small displacement method. When planetesimals undergo evaporation in the presence of nebular H_2 under a total pressure of approximately 10^{-4} bar, previous numerical simulations (*30*) demonstrate that the net isotope fractionation will be equal to the equilibrium isotope fractionation between vapor and melt. Thus, the Se and Te isotope fractionation between vapor and silicate melt during planetesimal evaporation can be derived from the <*F*> difference between vapor and silicate melt using Eq. 3.

Isotope fractionation during planetesimal evaporation and core formation

Similar to S, Se, and Te would have undergone violent vaporization during planetary accretion. We use the residual Se fraction (f_{res}) to describe the degree of Se loss during planetesimal evaporation. The Se concentration of planetesimals that formed proto-Earth (C_{BP}) after evaporation is $C_{BP} = C_{init} \times f_{res}$, where C_{init} refers to the initial Se concentration of the building material. Following a Rayleigh distillation model, the Se isotope composition of the bulk planetary embryo ($\delta^{82/76}Se_{BP}$) after evaporation is given by

$$\delta^{82/76}Se_{BP} = \delta^{82/76}Se_{init} + \Delta^{82/76}Se_{vapor-melt} \times \ln(f_{res}) \quad (5)$$

where $\delta^{82/76}Se_{init}$ is the initial Se isotope composition of building material and $\Delta^{82/76}Se_{vapor\text{-}melt}$ is the net Se isotope fractionation between vapor and melt. When the nebular H_2 is present under a total pressure of approximately 10^{-4} bar, the $\Delta^{82/76}Se_{vapor\text{-}melt}$ will be equal to the $10^3\ln\alpha_{vapor\text{-}silicate}$ of $^{82}Se/^{76}Se$.

During core formation, a large amount of Se would be segregated into the metallic core. Equilibrium between the core and mantle is given by the Se partition coefficient between metallic and silicate melts (*13*)

$$D_{Se}^{metal-silicate} = C_{core}/C_{BS} \quad (6)$$

where C_{BS} and C_{core} represent the Se concentrations in the bulk silicate part and core, respectively. On the basis of the mass balance, the total mass of Se in a bulk planet is conserved in these two reservoirs

$$C_{BP} = M_{BS} \times C_{BS} + (1 - M_{BS}) \times C_{core} \quad (7)$$

where M_{BS} is the mass fraction of the bulk silicate part. Following the Rayleigh distillation model, the Se isotope composition of the bulk silicate part ($\delta^{82/76}Se_{BS}$) is given by

$$\delta^{82/76}Se_{BS} = \delta^{82/76}Se_{BP} - 10^3\ln\alpha_{silicate-metal} \times \ln(f_{BS}) \quad (8)$$

where $10^3\ln\alpha_{silicate\text{-}metal}$ is the equilibrium Se isotope fractionation between silicate and metallic melts. f_{BS} is the Se fraction remaining in the bulk silicate reservoirs, which can be derived from Eqs. 6 and 7. If adopting the equilibrium model, then the $\delta^{82/76}Se_{BS}$ can be written as

$$\delta^{82/76}Se_{BS} = \delta^{82/76}Se_{BP} + (1 - f_{BS}) \times 10^3\ln\alpha_{silicate-metal} \quad (9)$$

By substituting the data of Te for those of Se, the abundance and isotopic composition of Te in the bulk silicate reservoir can be also derived using Eqs. 5 to 9.

Monte Carlo simulations for the isotope compositions of the bulk silicate reservoir

Our models do not require a late veneer, but a late addition of S, Se, and Te is still allowed if these elements undergo serious evaporative loss, e.g., their residual fractions are lower than 10%. In this case, the bulk silicate reservoir may have S, Se, and Te abundances lower than the present-day BSE's values after early planetesimal evaporation followed by late-stage core formation, and late delivery of S, Se, and Te is required to promote the abundances to the present-day values. Meanwhile, the S, Se, and Te isotope compositions of the bulk silicate reservoir would be also affected by the late veneer.

Here, we conducted Monte Carlo simulations to show how the S, Se, and Te isotope compositions of the bulk silicate reservoir are affected by the late veneer. The initial $\delta^{34/32}S$, $\delta^{82/76}Se$, and $\delta^{128/126}Te$ of the building material (71% enstatite chondrite + 24% ordinary chondrite + 5% carbonaceous chondrite) (*20*) are set as ~−0.21, −0.35, and, +0.02‰, respectively. The initial S, Se, and Te abundances in the build material are set as ~3.3 to 5.8 weight % (wt %), 15 to 25 parts per million (ppm) (*3*), and 1.6 to 2.3 ppm (*18*, *19*), respectively. $D_S^{metal/silicate}$, $D_{Se}^{metal/silicate}$, and $D_{Te}^{metal/silicate}$ during core formation range from 30 to 120. The residual fractions of S, Se, and Te after planetesimal evaporation, which measure the evaporation effect on the abundances, range from 0.01 to 0.2. The input parameters are randomly distributed in these ranges. The $\delta^{34/32}S$, $\delta^{82/76}Se$, and $\delta^{128/126}Te$ of the bulk silicate reservoir after early planetesimal evaporation followed by late-stage core formation are mainly affected by the evaporation process because core formation does not notably fractionate S, Se, and Te isotopes. Some input combinations produce the S, Se, and Te abundances in the bulk silicate reservoir exceeding the present-day BSE's values after planetesimal evaporation followed by core formation. These cases are ruled out as they cannot reproduce the S, Se, and Te abundances in the present-day BSE, regardless of the late-veneer effect. When the S, Se, and Te abundances in the bulk silicate reservoir are lower than the present-day BSE's values after planetesimal evaporation followed by core formation, a late veneer is required to increase their abundances to the present-day BSE's values. Meanwhile, the $\delta^{34/32}S$, $\delta^{82/76}Se$, and $\delta^{128/126}Te$ of the bulk silicate reservoir will be changed by the late veneer, which is characterized by the carbonaceous chondrite (fig. S1). The less S, Se, and Te remain after accretion, the more S, Se, and Te are required to be added by the late veneer, and the $\delta^{34/32}S$, $\delta^{82/76}Se$, and $\delta^{128/126}Te$ of the bulk silicate reservoir are closer to those of late-veneer material.

Supplementary Materials

This PDF file includes:

Supplementary Text
Figs. S1 to S9
References

REFERENCES AND NOTES

1. M. Schönbächler, R. W. Carlson, M. F. Horan, T. D. Mock, E. H. Hauri, Heterogeneous accretion and the moderately volatile element budget of earth. *Science* **328**, 884–887 (2010).
2. N. Braukmüller, F. Wombacher, C. Funk, C. Münker, Earth's volatile element depletion pattern inherited from a carbonaceous chondrite-like source. *Nat. Geosci.* **12**, 564–568 (2019).
3. Z. Wang, H. Becker, Ratios of S, Se and Te in the silicate Earth require a volatile-rich late veneer. *Nature* **499**, 328–331 (2013).
4. M. Fischer-Gödde, T. Kleine, Ruthenium isotopic evidence for an inner Solar System origin of the late veneer. *Nature* **541**, 525–527 (2017).
5. C.-L. Chou, Fractionation of siderophile elements in the Earths upper mantle. *Proc. Lunar Planet. Sci. Conf. 9th.* **1**, 219–230 (1978).
6. H. Becker, M. F. Horan, R. J. Walker, S. Gao, J.-P. Lorand, R. L. Rudnick, Highly siderophile element composition of the Earth's primitive upper mantle: Constraints from new data on peridotite massifs and xenoliths. *Geochim. Cosmochim. Acta* **70**, 4528–4550 (2006).
7. U. Mann, D. J. Frost, D. C. Rubie, H. Becker, A. Audétat, Partitioning of Ru, Rh, Pd, Re, Ir and Pt between liquid metal and silicate at high pressures and high temperatures—Implications for the origin of highly siderophile element concentrations in the Earth's mantle. *Geochim. Cosmochim. Acta* **84**, 593–613 (2012).

8. L. Rose-Weston, J. M. Brenan, Y. Fei, R. A. Secco, D. J. Frost, Effect of pressure, temperature, and oxygen fugacity on the metal-silicate partitioning of Te, Se, and S: Implications for earth differentiation. *Geochim. Cosmochim. Acta* **73**, 4598–4615 (2009).
9. A. Boujibar, D. Andrault, M. A. Bouhifd, N. Bolfan-Casanova, J. L. Devidal, N. Trcera, Metal-silicate partitioning of sulphur, new experimental and thermodynamic constraints on planetary accretion. *Earth Planet. Sci. Lett.* **391**, 42–54 (2014).
10. A. Yierpan, S. König, J. Labidi, R. Schoenberg, Selenium isotope and S-Se-Te elemental systematics along the Pacific-Antarctic ridge: Role of mantle processes. *Geochim. Cosmochim. Acta* **249**, 199–224 (2019).
11. R. A. Fischer, Y. Nakajima, A. J. Campbell, D. J. Frost, D. Harries, F. Langenhorst, N. Miyajima, K. Pollok, D. C. Rubie, High pressure metal–silicate partitioning of Ni, Co, V, Cr, Si, and O. *Geochim. Cosmochim. Acta* **167**, 177–194 (2015).
12. C. A. Norris, B. J. Wood, Earth's volatile contents established by melting and vaporization. *Nature* **549**, 507–510 (2017).
13. D. S. Grewal, R. Dasgupta, T. Hough, A. Farnell, Rates of protoplanetary accretion and differentiation set nitrogen budget of rocky planets. *Nat. Geosci.* **14**, 369–376 (2021).
14. R. A. Fischer, E. Cottrell, E. Hauri, K. K. M. Lee, M. Le Voyer, The carbon content of Earth and its core. *Proc. Natl. Acad. Sci.* **117**, 8743–8749 (2020).
15. J. Labidi, P. Cartigny, M. Moreira, Non-chondritic sulphur isotope composition of the terrestrial mantle. *Nature* **501**, 208–211 (2013).
16. J. Labidi, P. Cartigny, C. Hamelin, M. Moreira, L. Dosso, Sulfur isotope budget (^{32}S, ^{33}S, ^{34}S and ^{36}S) in Pacific-Antarctic ridge basalts: A record of mantle source heterogeneity and hydrothermal sulfide assimilation. *Geochim. Cosmochim. Acta* **133**, 47–67 (2014).
17. M. I. Varas-Reus, S. König, A. Yierpan, J.-P. Lorand, R. Schoenberg, Selenium isotopes as tracers of a late volatile contribution to Earth from the outer Solar System. *Nat. Geosci.* **12**, 779–782 (2019).
18. J. L. Hellmann, T. Hopp, C. Burkhardt, T. Kleine, Origin of volatile element depletion among carbonaceous chondrites. *Earth Planet. Sci. Lett.* **549**, 116508 (2020).
19. J. L. Hellmann, T. Hopp, C. Burkhardt, H. Becker, M. Fischer-Gödde, T. Kleine, Tellurium isotope cosmochemistry: Implications for volatile fractionation in chondrite parent bodies and origin of the late veneer. *Geochim. Cosmochim. Acta* **309**, 313–328 (2021).
20. N. Dauphas, The isotopic nature of the Earth's accreting material through time. *Nature* **541**, 521–524 (2017).
21. W. Wang, C. H. Li, J. P. Brodholt, S. Huang, M. J. Walter, M. Li, Z. Wu, F. Huang, S. J. Wang, Sulfur isotopic signature of Earth established by planetesimal volatile evaporation. *Nat. Geosci.* **14**, 806–811 (2021).
22. K. Lodders, Solar System Abundances and Condensation Temperatures of the Elements. *Astrophys. J.* **591**, 1220–1247 (2003).
23. B. J. Wood, D. J. Smythe, T. Harrison, The condensation temperatures of the elements: A reappraisal. *Am. Mineral.* **104**, 844–856 (2019).
24. W. M. Nash, D. J. Smythe, B. J. Wood, Compositional and temperature effects on sulfur speciation and solubility in silicate melts. *Earth Planet. Sci. Lett.* **507**, 187–198 (2019).
25. P. J. Jugo, M. Wilke, R. E. Botcharnikov, Sulfur K-edge XANES analysis of natural and synthetic basaltic glasses: Implications for S speciation and S content as function of oxygen fugacity. *Geochim. Cosmochim. Acta* **74**, 5926–5938 (2010).
26. M. Wadhwa, Redox conditions on small bodies, the Moon and Mars. *Rev. Mineral. Geochemistry.* **68**, 493–510 (2008).
27. J. Wade, B. J. Wood, Core formation and the oxidation state of the Earth. *Earth Planet. Sci. Lett.* **236**, 78–95 (2005).
28. J. Bigeleisen, M. G. Mayer, Calculation of Equilibrium Constants for Isotopic Exchange Reactions. *J. Chem. Phys.* **15**, 261–267 (1947).
29. T.-A. Suer, J. Siebert, L. Remusat, N. Menguy, G. Fiquet, A sulfur-poor terrestrial core inferred from metal–silicate partitioning experiments. *Earth Planet. Sci. Lett.* **469**, 84–97 (2017).
30. E. D. Young, A. Shahar, F. Nimmo, H. E. Schlichting, E. A. Schauble, H. Tang, J. Labidi, Near-equilibrium isotope fractionation during planetesimal evaporation. *Icarus.* **323**, 1–15 (2019).
31. H. Tang, E. D. Young, Evaporation from the Lunar Magma Ocean Was Not the Mechanism for Fractionation of the Moon's Moderately Volatile Elements. *Planet. Sci. J.* **1**, 49 (2020).
32. R. Martins, S. Kuthning, B. J. Coles, K. Kreissig, M. Rehkämper, Nucleosynthetic isotope anomalies of zinc in meteorites constrain the origin of Earth's volatiles. *Science* **379**, 369–372 (2023).
33. N. X. Nie, D. Wang, Z. A. Torrano, R. W. Carlson, C. M. O'D. Alexander, A. Shahar, Meteorites have inherited nucleosynthetic anomalies of potassium-40 produced in supernovae. *Science* **379**, 372–376 (2023).
34. T. Steller, C. Burkhardt, C. Yang, T. Kleine, Nucleosynthetic zinc isotope anomalies reveal a dual origin of terrestrial volatiles. *Icarus.* **386**, 115171 (2022).
35. P. S. Savage, F. Moynier, M. Boyet, Zinc isotope anomalies in primitive meteorites identify the outer solar system as an important source of Earth's volatile inventory. *Icarus.* **386**, 115172 (2022).
36. J. Render, M. Fischer-Gödde, C. Burkhardt, T. Kleine, The cosmic molybdenum-neodymium isotope correlation and the building material of the Earth. *Geochemical Perspect. Lett.* **3**, 170–178 (2017).
37. G. Budde, C. Burkhardt, T. Kleine, Molybdenum isotopic evidence for the late accretion of outer Solar System material to Earth. *Nat. Astron.* **3**, 736–741 (2019).
38. S. Johnston, A. Brandon, C. McLeod, K. Rankenburg, H. Becker, P. Copeland, Nd isotope variation between the Earth–Moon system and enstatite chondrites. *Nature* **611**, 501–506 (2022).
39. M. Schiller, M. Bizzarro, J. Siebert, Iron isotope evidence for very rapid accretion and differentiation of the proto-Earth. *Sci. Adv.* **6**, eaay7604 (2020).
40. T. Hopp, N. Dauphas, F. Spitzer, C. Burkhardt, T. Kleine, Earth's accretion inferred from iron isotopic anomalies of supernova nuclear statistical equilibrium origin. *Earth Planet. Sci. Lett.* **577**, 117245 (2022).
41. A. Trinquier, J.-L. Birck, C. J. Allegre, Widespread ^{54}Cr Heterogeneity in the Inner Solar System. *Astrophys. J.* **655**, 1179–1185 (2007).
42. S.-J. Wang, W. Wang, J.-M. Zhu, Z. Wu, J. Liu, G. Han, F.-Z. Teng, S. Huang, H. Wu, Y. Wang, G. Wu, W. Li, Nickel isotopic evidence for late-stage accretion of Mercury-like differentiated planetary embryos. *Nat. Commun.* **12**, 294 (2021).
43. L. Qin, C. M. O'D. Alexander, R. W. Carlson, M. F. Horan, T. Yokoyama, Contributors to chromium isotope variation of meteorites. *Geochim. Cosmochim. Acta* **74**, 1122–1145 (2010).
44. N. Braukmüller, F. Wombacher, D. C. Hezel, R. Escoube, C. Münker, The chemical composition of carbonaceous chondrites: Implications for volatile element depletion, complementarity and alteration. *Geochim. Cosmochim. Acta* **239**, 17–48 (2018).
45. M. M. Hirschmann, Comparative deep Earth volatile cycles: The case for C recycling from exosphere/mantle fractionation of major (H2O, C, N) volatiles and from H2O/Ce, CO2/Ba, and CO2/Nb exosphere ratios. *Earth Planet. Sci. Lett.* **502**, 262–273 (2018).
46. C. M. O'D. Alexander, R. Bowden, M. L. Fogel, K. T. Howard, C. D. K. Herd, L. R. Nittler, The provenances of asteroids, and their contributions to the volatile inventories of the terrestrial planets. *Science* **337**, 721–723 (2012).
47. H. Palme, H. S. C. O'Neill, in *Treatise on Geochemistry* (Elsevier, ed. 2, 2014), pp. 1–39.
48. W. Wang, M. J. Walter, Y. Peng, S. Redfern, Z. Wu, Constraining olivine abundance and water content of the mantle at the 410-km discontinuity from the elasticity of olivine and wadsleyite. *Earth Planet. Sci. Lett.* **519**, 1–11 (2019).
49. W. Wang, H. Zhang, J. P. Brodholt, Z. Wu, Elasticity of hydrous ringwoodite at mantle conditions: Implication for water distribution in the lowermost mantle transition zone. *Earth Planet. Sci. Lett.* **554**, 116626 (2020).
50. W. Wang, Y. Li, J. P. Brodholt, L. Vočadlo, M. J. Walter, Z. Wu, Strong shear softening induced by superionic hydrogen in Earth's inner core. *Earth Planet. Sci. Lett.* **568**, 117014 (2021).
51. L. Piani, Y. Marrocchi, T. Rigaudier, L. G. Vacher, D. Thomassin, B. Marty, Earth's water may have been inherited from material similar to enstatite chondrite meteorites. *Science* **369**, 1110–1113 (2020).
52. E. D. Young, A. Shahar, H. E. Schlichting, Earth shaped by primordial H2 atmospheres. *Nature* **616**, 306–311 (2023).
53. P. A. Sossi, O. Nebel, H. S. C. O'Neill, F. Moynier, Zinc isotope composition of the Earth and its behaviour during planetary accretion. *Chem. Geol.* **477**, 73–84 (2018).
54. P. S. Savage, F. Moynier, H. Chen, G. Shofner, J. Siebert, J. Badro, I. S. Puchtel, Copper isotope evidence for large-scale sulphide fractionation during Earth's differentiation. *Geochemical Perspect. Lett.* **1**, 53–64 (2015).
55. B. Marty, The origins and concentrations of water, carbon, nitrogen and noble gases on Earth. *Earth Planet. Sci. Lett.* **313–314**, 56–66 (2012).
56. D. S. Grewal, R. Dasgupta, C. Sun, K. Tsuno, G. Costin, Delivery of carbon, nitrogen, and sulfur to the silicate Earth by a giant impact. *Sci. Adv.* **5**, eaau3669 (2019).
57. K. Righter, M. Humayun, L. Danielson, Partitioning of palladium at high pressures and temperatures during core formation. *Nat. Geosci.* **1**, 321–323 (2008).
58. T.-A. Suer, J. Siebert, L. Remusat, J. M. D. Day, S. Borensztajn, B. Doisneau, G. Fiquet, Reconciling metal–silicate partitioning and late accretion in the Earth. *Nat. Commun.* **12**, 2913 (2021).
59. P. Richet, Y. Bottinga, M. Javoy, A review of hydrogen, carbon, nitrogen, oxygen, sulphur, and chlorine stable isotope fractionation among gaseous molecules. *Annu. Rev. Earth Planet. Sci.* **5**, 65–110 (1977).
60. W. Wang, Z. Wu, F. Huang, Equilibrium barium isotope fractionation between minerals and aqueous solution from first-principles calculations. *Geochim. Cosmochim. Acta* **292**, 64–77 (2021).
61. P. E. Blöchl, Projector augmented-wave method. *Phys. Rev. B.* **50**, 17953–17979 (1994).
62. J. P. Perdew, K. Burke, M. Ernzerhof, Generalized gradient approximation made simple. *Phys. Rev. Lett.* **77**, 3865–3868 (1996).
63. R. Caracas, K. Hirose, R. Nomura, M. D. Ballmer, Melt–crystal density crossover in a deep magma ocean. *Earth Planet. Sci. Lett.* **516**, 202–211 (2019).

64. M. I. Petaev, The GRAINS thermodynamic and kinetic code for modeling nebular condensation. *CALPHAD* **33**, 317–327 (2009).
65. Z. D. Sharp, Nebular ingassing as a source of volatiles to the Terrestrial planets. *Chem. Geol.* **448**, 137–150 (2017).
66. A. Yierpan, S. König, J. Labidi, T. Kurzawa, M. G. Babechuk, R. Schoenberg, Chemical Sample Processing for Combined Selenium Isotope and Selenium-Tellurium Elemental Investigation of the Earth's Igneous Reservoirs. *Geochemistry, Geophys. Geosystems.* **19**, 516–533 (2018).
67. C. Defouilloy, P. Cartigny, N. Assayag, F. Moynier, J.-A. Barrat, High-precision sulfur isotope composition of enstatite meteorites and implications of the formation and evolution of their parent bodies. *Geochim. Cosmochim. Acta* **172**, 393–409 (2016).
68. X. Gao, M. H. Thiemens, Isotopic composition and concentration of sulfur in carbonaceous chondrites. *Geochim. Cosmochim. Acta* **57**, 3159–3169 (1993).
69. X. Gao, M. H. Thiemens, Variations of the isotopic composition of sulfur in enstatite and ordinary chondrites. *Geochim. Cosmochim. Acta* **57**, 3171–3176 (1993).
70. J. Labidi, J. Farquhar, C. M. O'D. Alexander, D. L. Eldridge, H. Oduro, Mass independent sulfur isotope signatures in CMs: Implications for sulfur chemistry in the early solar system. *Geochim. Cosmochim. Acta* **196**, 326–350 (2017).
71. J. Labidi, S. König, T. Kurzawa, A. Yierpan, R. Schoenberg, The selenium isotopic variations in chondrites are mass-dependent; Implications for sulfide formation in the early solar system. *Earth Planet. Sci. Lett.* **481**, 212–222 (2018).

Acknowledgments: We thank B. Fegley for constructive discussion. **Funding:** This study is supported by the National Natural Science Foundation of China (41925017 and 41721002), Chinese Academy of Sciences Hundred Talents Program, and the UCL-Carnegie Postdoctoral Scholarship. S. H. acknowledges support from NSF (AST-1910955 and EAR-2244895). M.P. acknowledges support from DOE grant (DE-NA0004084). First-principle calculations were conducted at the Supercomputing Center of the University of Science and Technology of China.
Author contributions: Conceptualization: W.W. Methodology: W.W. and M.I.P. Investigation: W. W. Visualization: W.W. Supervision: W.W., M.J.W., J.P.B., and S.H. Writing—original draft: W.W. Writing—review and editing: W.W., M.J.W., J.P.B., S.H., and M.I.P. **Competing interests:** The authors declare that they have no competing interests. **Data and materials availability:** All data needed to evaluate the conclusions in the paper are present in the paper and/or the Supplementary Materials. The Vienna Ab Initio Simulation Package is a commercial software available for purchase at www.vasp.at/.

Submitted 8 February 2023
Accepted 7 November 2023
Published 6 December 2023
10.1126/sciadv.adh0670

ScienceAdvances

Chalcogen isotopes reveal limited volatile contribution from late veneer to Earth

Wenzhong Wang, Michael J. Walter, John P. Brodholt, Shichun Huang, and Michail I. Petaev

Sci. Adv. **9** (49), eadh0670. DOI: 10.1126/sciadv.adh0670

Science Advances (ISSN 2375-2548) is published by the American Association for the Advancement of Science. 1200 New York Avenue NW, Washington, DC 20005. The title *Science Advances* is a registered trademark of AAAS.